energies

MDPI

Article

Synergies between Direct Air Capture Technologies and Solar Thermochemical Cycles in the Production of Methanol

Enric Prats-Salvado [1,2,*], Nathalie Monnerie [1] and Christian Sattler [1,2]

[1] German Aerospace Center (DLR), Institute of Future Fuels, 51147 Cologne, Germany; nathalie.monnerie@dlr.de (N.M.); Christian.Sattler@dlr.de (C.S.)
[2] Faculty of Mechanical Science and Engineering, Institute of Power Engineering, Solar Fuel Production, TU Dresden, 01062 Dresden, Germany
* Correspondence: enric.pratssalvado@dlr.de; Tel.: +49-2203-601-2624

Abstract: Methanol is an example of a valuable chemical that can be produced from water and carbon dioxide through a chemical process that is fully powered by concentrated solar thermal energy and involves three steps: direct air capture (DAC), thermochemical splitting and methanol synthesis. In the present work, we consider the whole value chain from the harvesting of raw materials to the final product. We also identify synergies between the aforementioned steps and collect them in five possible scenarios aimed to reduce the specific energy consumption. To assess the scenarios, we combined data from low and high temperature DAC with an Aspen Plus® model of a plant that includes water and carbon dioxide splitting units via thermochemical cycles (TCC), CO/CO_2 separation, storage and methanol synthesis. We paid special attention to the energy required for the generation of low oxygen partial pressures in the reduction step of the TCC, as well as the overall water consumption. Results show that suggested synergies, in particular, co-generation, are effective and can lead to solar-to-fuel efficiencies up to 10.2% (compared to the 8.8% baseline). In addition, we appoint vacuum as the most adequate strategy for obtaining low oxygen partial pressures.

Keywords: thermochemical cycles; direct air capture; methanol production; process integration; solar energy

Citation: Prats-Salvado, E.; Monnerie, N.; Sattler, C. Synergies between Direct Air Capture Technologies and Solar Thermochemical Cycles in the Production of Methanol. *Energies* **2021**, *14*, 4818. https://doi.org/10.3390/en14164818

Academic Editor: John Boland

Received: 30 June 2021
Accepted: 28 July 2021
Published: 7 August 2021

1. Introduction

It is a well-known fact that the emissions of CO_2 and other global warming gases have increased steadily since the industrial revolution due to the strong and undeniable energetic dependency of humanity on fossil fuels. According to available studies, the so-called anthropogenic emissions are the responsible of a sharp increase in CO_2 atmospheric levels to unprecedented values in the last 800,000 years [1]. While the connection between CO_2 and a climatic change was formulated more than 60 years ago [2], it is nowadays evidenced across the globe in manifold forms. High-temperature anomalies on land and sea, thinner ice cover in polar regions or the general retreat of glaciers are just some of the consequences [3]. These disturbances are posing increasing challenges to humanity such as food insecurity, air pollution or endangered water access. It is not surprising that these issues will take a heavier toll on the most vulnerable communities [4]. In front of this scenario, governments and policymakers are called to act in order to bridge the emissions gap. This gap can be defined as the difference between the current situation and the desired emission levels to achieve a global warming below 2 °C, as stated in the Paris Agreement [5].

The present study focuses on two technologies that can contribute to tackle global warming: synthetic fuels production with solar energy and negative carbon emissions. Traditionally, research has been centered either in carbon capture processes or synthetic fuels production. This work follows the path outlined by recent studies [6,7] and bridges the gaps between both technologies by exploring in more detail the potential synergies

that could develop in a future ecosystem. Due to their novelty, many combinations are possible, and to the best knowledge of the authors, they have not been assessed to the date. Therefore, the objective of this analysis is providing a set of recommendations that could help future researchers to focus and/or discard some concepts already proven to be suboptimal.

A synthetic fuel can be defined as a liquid fuel produced from the energetic upgrade of low energy feedstocks such as water or carbon dioxide [8]. When renewable energies such as solar are used to re-energize these raw materials, synthetic fuels can be considered carbon-neutral (i.e., the total amount of global warming gases released during their production and consumption is zero). Synthetic fuels could become an asset for decarbonizing transportation, but also for providing chemical industry with climate-neutral feedstocks [9]. At the same time, they can contribute to the storage of electricity surpluses from the grid during peak production of renewable energies, providing a long-term storage of electricity [10]. In the transport sector, synthetic fuels could be combined with electrification, which is an effective way to decarbonize light vehicles, but certainly not an alternative for heavy duty transportation [11]. Given that the chemical industry strongly relies on fossil fuels, both as a feedstock and as an energy source, the introduction of synthetic fuels could substantially improve its sustainability. Already available chemical routes can supply a wide range of raw materials, including methane, methanol or even synthetic crude oil [8,12]. Therefore, the transition could be possible without costly modifications on available infrastructure or final products. Methanol is an interesting commodity chemical due to its already widespread use as a fuel for internal combustion engines and chemical industry feedstocks [13,14], and thus, it is chosen as the final product for the processes described in this study. To produce methanol, carbon monoxide and hydrogen are commonly used as raw materials. These reactants are traditionally obtained from fossil resources via coal gasification or steam methane reforming. Nevertheless, green pathways are also available and are based in one of the three following options: (1) water splitting to hydrogen (WS) with reverse water-gas shift, (2) carbon dioxide splitting to carbon monoxide (CDS) with water-gas shift or (3) a combination of water and carbon dioxide splitting (also known as co-splitting). The suggested process in this study relies on the third option since previous research show that this is the most efficient pathway [15].

The WS and CDS reactions are performed with a thermochemical cycle (TCC). These cycles involve a metal oxide redox pair and use concentrated solar thermal energy (CSTE) as a heat source [8]. They are capable of performing WS and CDS reactions at considerably lower temperatures than direct thermolysis, which is not possible below 3000 °C due to thermodynamic constraints [12]. The chosen metal oxide for the TCC in this work is ceria oxide, since it is one of the most promising materials [16,17]. The reactions involved are an oxidation and a reduction performed at different temperatures. Equations (1) and (2) show the oxidation reaction for water and carbon dioxide splitting, respectively, while Equation (3) is common for both compounds. A non-stoichiometry index is used to show the reduction and oxidation extent (δ_{red} and δ_{ox}, respectively). In order to enhance the hydrogen yield per mole of ceria oxide ($\Delta\delta$), δ_{ox} must be minimized while maximizing δ_{red}. The former is thermodynamically favored by low temperatures, although kinetics can become a bottleneck below 700 to 1000 °C [8]. The latter is increased through high temperatures (technically feasible up to 1500 °C) and as low oxygen partial pressure as possible, which can be achieved by vacuum or sweep gas [18]. The relationship at 1500 °C between the oxygen partial pressure and the reduction extent can be observed in Figure 1. In the plot, the required amount of ceria per mole of hydrogen produced is also depicted. Although not being technically challenging, production of high vacuum and large sweep gas flows can compromise the economic feasibility of the system [19,20]. For this reason, this auxiliary process has also been studied and will be described in Section 2.3.1.

$$CeO_{2-\delta_{red}} + \Delta\delta\ H_2O \rightarrow CeO_{2-\delta_{ox}} + \Delta\delta\ H_2 \quad (1)$$

$$CeO_{2-\delta_{red}} + \Delta\delta\ CO_2 \rightarrow CeO_{2-\delta_{ox}} + \Delta\delta\ CO \quad (2)$$

$$CeO_{2-\delta_{ox}} \rightarrow CeO_{2-\delta_{red}} + \frac{\Delta\delta}{2} O_2 \quad (3)$$

$$\Delta\delta = \delta_{red} - \delta_{ox} \quad (4)$$

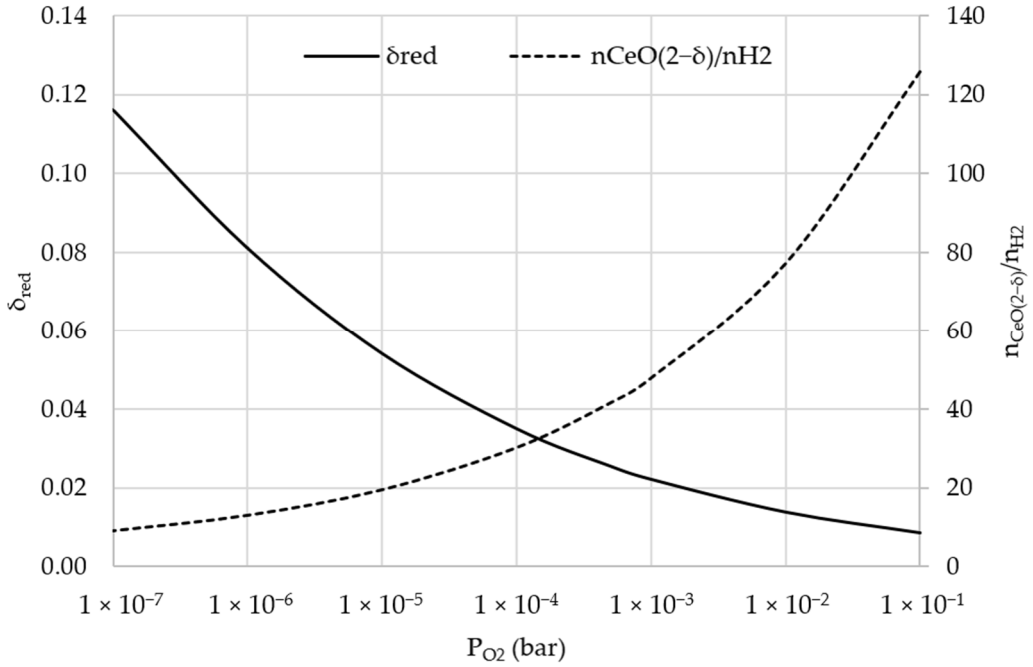

Figure 1. Dependency at 1500 °C between oxygen partial pressure (P_{O2}) and reduction extent (δ_{red}, left axis) and quantity of ceria per mole of hydrogen ($n_{CeO(2-\delta)}/n_{H2}$, right axis) according to Bulfin et al. [21].

As previously mentioned, TCC are powered by CSTE, which is an established renewable energy that uses Direct Normal Irradiation (DNI) as a heat source. Although it is vastly used for electricity production worldwide, it can also supply process heat at temperatures up to 2300 K [22,23]. Since thermochemical cycles require substantially high temperatures, high concentrations ratios are preferred and therefore, point-focus receivers will be used [24]. The biggest potential of CSTE is achieved in areas with direct normal irradiation above 2000 kWh/m^2/y. These areas tend mostly to be concentrated in desert regions and as a consequence, water consumption must be carefully monitored [25]. By obtaining the needed energy from CSTE, higher efficiencies and much lower footprints are expected if TCC are compared to electrolysis pathways and biomass-based approach [11]. In addition, solar energy is claimed to be the only renewable energy with enough capacity to power the difficult endeavor of replacing fossil fuels [26].

Negative carbon emissions are considered as part of the solution by the Paris Agreement, especially in the second half of the current century, when the net emissions of global warming gases are expected to be zero [5]. This means that carbon dioxide must be removed from natural sinks (e.g., atmosphere, oceans or vegetation) and either used as a raw material for fuels or chemicals (also known as "carbon capture and utilization" or CCU) or sequestrated elsewhere (commonly named "carbon capture and storage" or CCS). The former approach is a perfect match for the aforementioned production of synthetic fuels because it allows for closing the carbon cycle: CO_2 emitted in the combustion is collected and recycled as a feedstock [27,28]. Although recent works on indirect ocean carbon capture have shown promising results [29,30], direct air capture (DAC) and biomass-based concepts stand out as the most mature approaches. However, the scalability of DAC has proven higher than biomass-based methods due to a much more reduced land footprint, even if considering the area needed for harvesting the required renewable energy [28,31]. Therefore, DAC will be the preferred carbon capture method in this study. Based on available literature,

two different processes have been chosen for the DAC section: high temperature aqueous solutions (HT-DAC) and low temperature solid sorbents (LT-DAC) [31]. In addition, a third process has been suggested in this study consisting of a variation of the HT-DAC powered by CSTE and named "sHT-DAC".

HT-DAC relies on two cycles operated in a continuous way. In the first cycle, atmospheric air without specified pre-treatment contacts a sprayed potassium hydroxide solution, allowing CO_2 to react with it and producing potassium carbonate Equation (5). The obtained solution is fed in a regeneration reactor with calcium hydroxide, thus leading to calcium carbonate and potassium hydroxide Equation (6). At this point the second cycle begins by removing the calcium carbonate pellets and calcining them at high temperatures (900 °C). The products of this decomposition are pure CO_2 and calcium oxide Equation (7), which is slacked (i.e., mixed with water to produce calcium hydroxide) Equation (8) and recycled to the regeneration reactor. The main energy inputs required by this system are the forced air circulation to the contactor and the heat for the calcination step, which is supplied by the combustion of natural gas with pure oxygen (oxyfuel), although a fully electric approach is claimed to be under development. The emitted CO_2 is also collected and is part of the captured gas stream [31,32].

$$2\,KOH + CO_2 \rightarrow K_2CO_3 + H_2O \quad (5)$$

$$K_2CO_3 + Ca(OH)_2 \rightarrow 2\,KOH + CaCO_3 \quad (6)$$

$$CaCO_3 \rightarrow CaO + CO_2 \quad (7)$$

$$CaO + H_2O \rightarrow Ca(OH)_2 \quad (8)$$

In LT-DAC, absorption and desorption take place sequentially in a single unit that typically contains amines fixed on a solid support, although other compounds have also been reported. Non-treated atmospheric air is fed through these units, and CO_2 is captured until the sorbent material is saturated. Then, the unit is isolated and regenerated through vacuum and heat, which can be provided by steam at low temperatures (100 °C). Most relevant energetic consumers in this process are also air pumping and the desorption step. However, the low temperatures of the latter allow the usage of waste heat from other industrial processes [31,33]. Moreover, low temperatures allow the integration of LT-DAC with heating, ventilation and air conditioning (HVAC) systems. The benefit of this idea would be the energy savings on electricity, since vast amounts of air are already being pumped by HVAC systems across the world. Given that the LT-DAC units are typically compact and offer a small pressure drop, their addition to HVAC systems should be technically possible [6].

The last approach, sHT-DAC, is a modification of the HT-DAC in which the calcination step is performed with aid of CSTE instead of combustion or electric heating. This concept is inspired by previous works on solar rotary kilns for cement production, where exactly the same reaction takes place [34]. In Figure 2, the available data for HT- and LT-DAC approaches can be read. It should be noted, that compression of CO_2 to 150 bar is included in the electrical consumption, which can be approximated as 120 kWh/t CO_2 [32,35]. For the HT-DAC, the consumption of the air separation unit (ASU) is also considered.

Finally, the water consumption of DAC can vary substantially depending on the technology and the environmental conditions. On the one-hand, HT-DAC (and subsequently sHT-DAC) is claimed to have a consumption of 4.7 water tons per ton of captured CO_2 at 20 °C and 64% relative humidity due to the water evaporated in the contactor. However, this value can double at lower humidity and higher temperatures [32]. On the other hand, studies show that LT-DAC captures moisture from the air and thus, water is obtained from its operation with quantities around 1 ton of water per ton of captured CO_2 [36]. Notwithstanding, the energy consumption for the desorption of captured water is several orders of magnitude above desalination [37]. Therefore, water capture through LT-DAC is generally undesirable yet unavoidable.

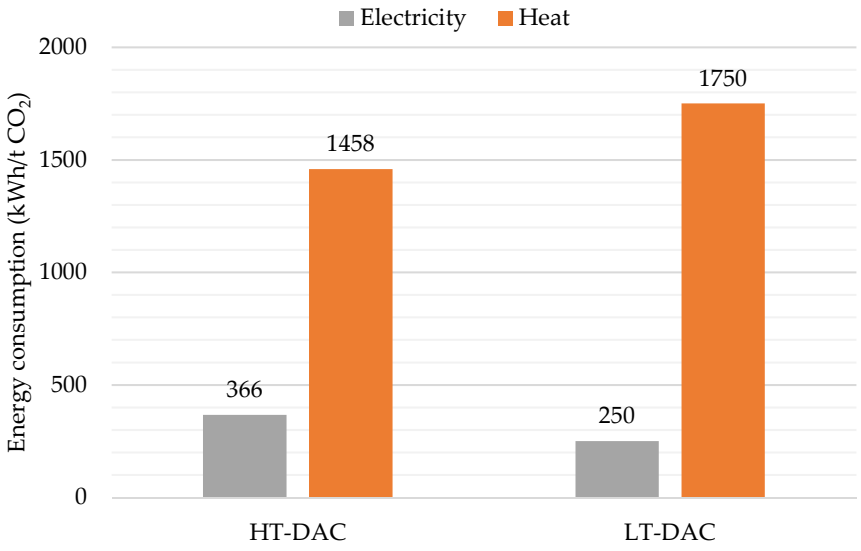

Figure 2. Comparison of the energy requirements per captured ton of CO_2 for each technology. Figures for high-temperature DAC (HT-DAC) and low temperature DAC (LT-DAC) are extracted from the works of Keith et al. [32] and Fasihi et al. [31], respectively. For those figures specified in ranges, the average value was taken.

Although not directly related with DAC nor quantified in this analysis, HVAC systems can also provide considerable amounts of water if condensation under humid environmental conditions is collected [38,39].

2. Methodology

In the current work, several approaches of DAC will be combined with an already demonstrated plant concept for methanol production through the splitting of water and carbon dioxide [15,40,41]. This concept is depicted in Figure 3.

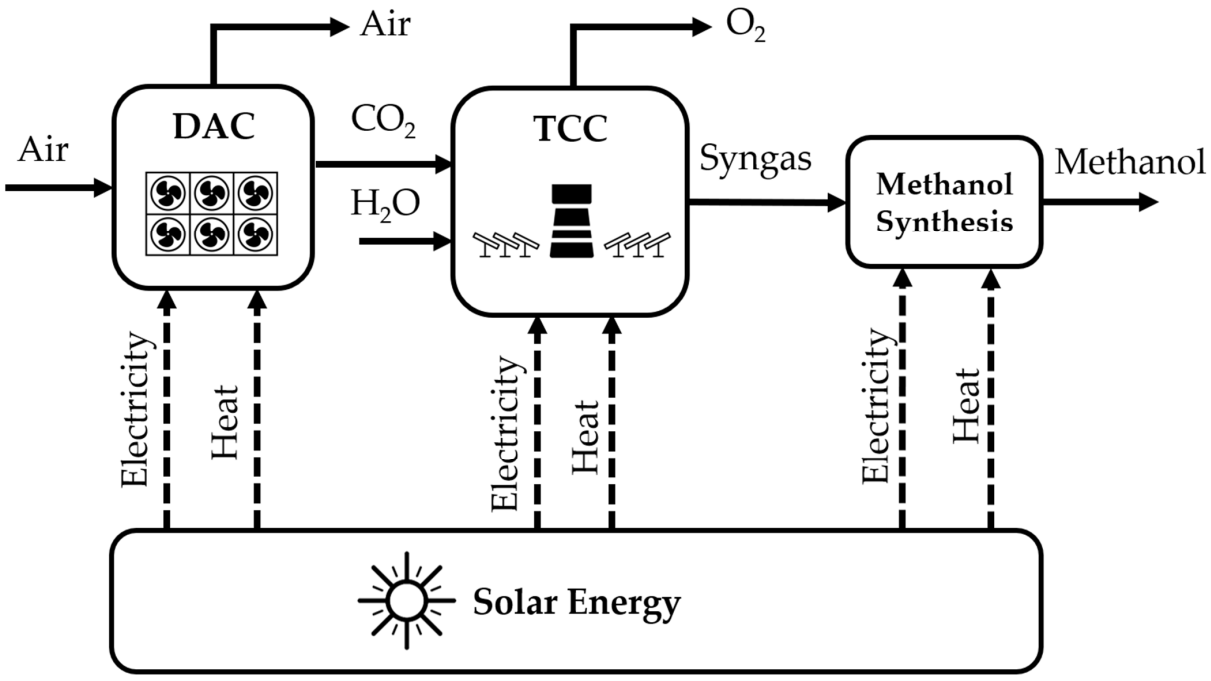

Figure 3. Schematic representation of the overall process. The acronyms DAC and TCC stand for direct air capture and thermochemical cycle, respectively.

2.1. Modelling of DAC

For the HT- and LT-DAC approaches, the available data in literature shown in Figure 2 has been directly used. The only modification required has been the subtraction of the compression work when the configuration did not require it. For the sHT-DAC approach, the detailed model available of the HT-DAC process [32] allowed the approximate calculation of the energy needs for such a system by only considering the calciner heat input. This assumption should be acceptable given that all the other units of the process are exothermal with much lower heat duties.

2.2. Modelling of TCC and Methanol Synthesis

In order to model the thermochemical cycle and the methanol synthesis, an Aspen Plus® simulation with both of them was built. The physical parameters of the involved compounds were retrieved from APV100.PURE36 and APV100.INORGANIC Databanks, while the property method used was "Electrolyte NRTL with Redlich-Kwong equation of state" (ELECNRTL). A simplified flow diagram of the whole production of synthetic fuel can be found in Figure 4, while the complete flowsheet and stream table are available in Supplementary Materials.

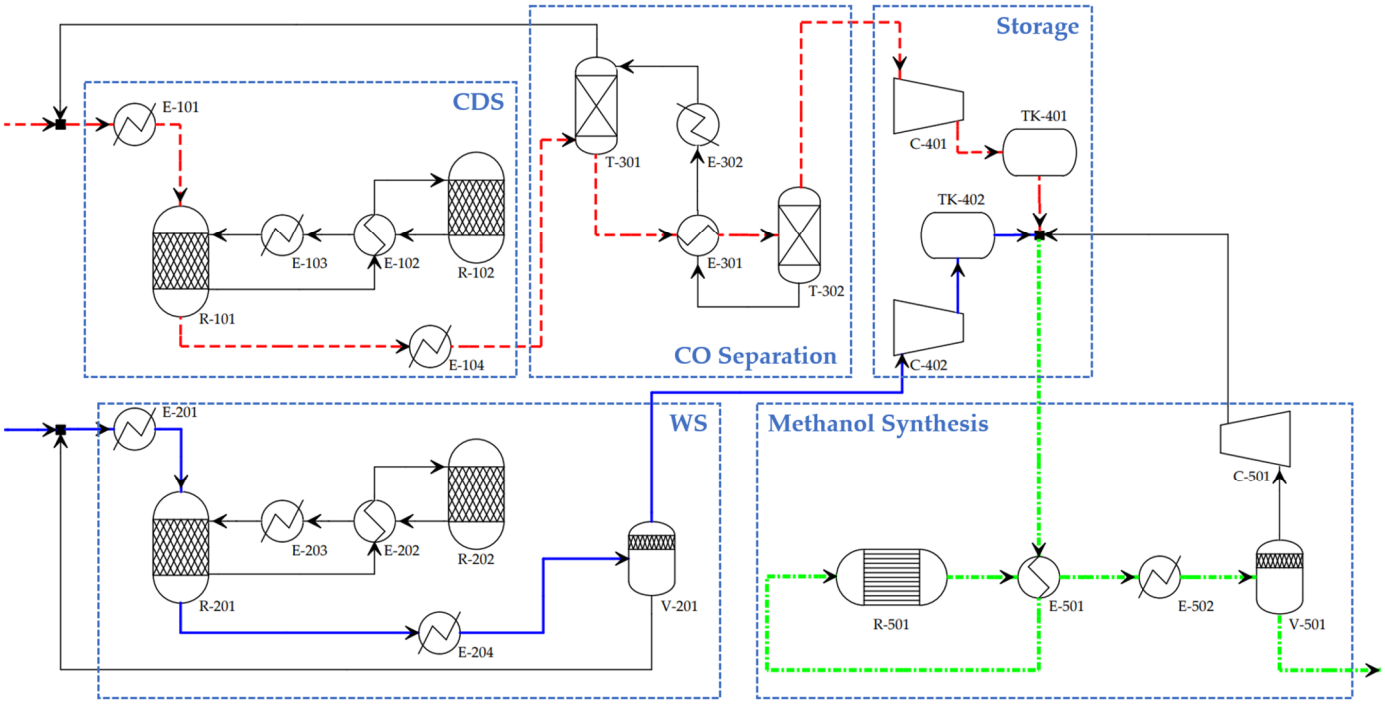

Figure 4. Simplified flowsheet of the methanol production process from water and carbon dioxide. The paths of H_2/H_2O and CO/CO_2 are shown with a red-dashed line and a blue-solid line, respectively, while the main path of methanol synthesis is depicted with a dashed-dotted line in green. The oxidation takes place in reactors R-101 and R-201, whereas the reduction of ceria is performed in reactors R-102 and R-202. Acronyms WS and CDS stand for water and carbon dioxide splitting, respectively.

The oxidation (R-101 and R-201) and reduction reactors (R-102 and R-202) are based on a layout from literature [22,42] and have been implemented in Aspen Plus® with the conversion reactor model (RStoic). For the feasibility of the process simulation with this software, the recommended arrangement performs the reduction and oxidation in different isothermal reactors, where temperature and pressure are constant, while the metal oxide is transferred between them. Since both reactors operate at considerably high temperatures (between 1500 and 900 °C), heat losses are not neglectable. As a consequence, the oxidation reactor is often operated without refrigeration even though reactions (1)

and (2) are exothermal and the reduction reactor must be irradiated with concentrated sunlight to compensate the endothermicity of reaction (3) and the heat losses [42]. To avoid simulation difficulties caused by different thermodynamic and kinetic properties, the equipment is duplicated to perform WS and CDS separately [18,43]. The work from Bulfin et al. was used to determine the oxidation and reduction extent as well as the H_2O or CO_2 conversion for each reactor [22]. The reaction conditions and other relevant variables for the simulation are shown in Table 1.

Table 1. Summary of conditions for reduction (R-102 and R-202) and oxidation reactors (R-101 and R-201). The conditions are identical for the oxidation with water and carbon dioxide, in exception of reaction extent (δ). It should be noted that δ refers to δ_{ox} for the oxidation reactor and δ_{red} for the reduction reactor.

Parameter	Oxidation (CO_2)	Oxidation (H_2O)	Reduction
Temperature	900 °C		1500 °C
Pressure	1 bar		0.5 mbar
Conversion	40%		40%
δ	1.37×10^{-3}	1.36×10^{-3}	0.0254

The gas outlet of the reactors is cooled down and products (H_2 and CO) are separated from reactants (H_2O and CO_2, respectively). The separation of water and hydrogen is performed by a series of flash tanks, while the mixture of CO and CO_2 must undergo a more complex process to be separated due to their low boiling points. The chosen technology in the final simulation is liquid absorption, but other alternatives have also been considered. According to literature, vacuum-pressure swing adsorption (VPSA) of carbon monoxide [44] could be a competitive alternative, while cryogenic distillation or membrane separation have too high energy consumptions [45–47]. In addition, the possibility of using the already available DAC equipment in order to remove the unreacted CO_2 is studied, which is a novel approach. To compare the different separation alternatives, the models described on literature for liquid absorption [48] and VPSA [47] were reproduced in the same Aspen Plus® simulation. Data shown in Figure 2 was used for quantifying energy needs of CO purification with DAC equipment.

As already described, the thermochemical cycle requires heat delivered by CSTE and thus, the WS and CDS depend on sunlight availability. However, the production of methanol from hydrogen and carbon monoxide is operated around the clock for operability and economic reasons: on the one hand, daily shutdowns are avoided, and on the other hand, the flowrates and the equipment can be smaller while obtaining the same output [40]. Consequently, a storing unit for the gases is needed (TK-401). The storing pressure is set to 50 bar, and H_2 and CO are stored separately to avoid corrosion issues caused by the combination of CO_2 and H_2O traces [49,50]. Downstream, methanol synthesis Equation (9) is performed at 50 bar and 250 °C in an isothermal catalytic reactor (R-501), which is also reproduced with the conversion reactor model (RStoic). Conversions of 50% per pass are assumed due to thermodynamic limitations [51]. The reaction also dictates the 2:1 ratio between H_2 and CO produced and, as a consequence, the WS section must double the CDS output in steady state.

$$2\,H_2 + CO \rightarrow CH_3OH \quad (9)$$

The outlet of the reactor is quenched, and non-reacted hydrogen and carbon monoxide are flashed and recycled. Finally, methanol is distilled to the desired purity grade (>99% in the current simulation).

2.3. Modelling of Auxiliary Equipment

2.3.1. Sweep Gas and Vacuum

Generating sweep gas and/or vacuum is of major importance for achieving low oxygen partial pressures that enhance the reduction of ceria oxide. The production of

high purity nitrogen (oxygen impurities below 1 ppm) is estimated to be 16 kJ/mol for a commercial cryogenic plant [52]. For calculating the energy consumption of the vacuum generation, the recommendations of several publications were followed and a system with steam jets coupled with a mechanical pump that achieved an oxygen partial pressure down to 5×10^{-4} bar is modelized [20,51]. In case of vacuums above 50 mbar, only the mechanical pump is required. The models for both systems were reproduced from relevant literature [53]. To find the optimal solution, these models were combined to perform a screening of energy costs for a range of reduction pressures (between 1 and 1×10^{-4} bar) and sweep gas purity (oxygen molar fractions between 0.1 and 1×10^{-4}).

A sensitivity analysis is performed to predict what could be the consequences of using an innovative approach based on a thermochemical oxygen pump. This concept, if coupled with the vacuum equipment presented in this study, could produce oxygen partial pressures as low as 1×10^{-6} bar without substantially increasing the energy consumption [21,54]. In the sensitivity analysis, it is assumed that this oxygen partial pressure can be reached without an additional energy consumption.

2.3.2. Heat Integration and Waste Heat Exploitation

As heat demand of both DAC and synthetic fuels production is considerably large, potential integration between the two processes is possible and desirable. While literature provided the net heat demand of DAC, energy needs had to be calculated for the production of methanol from CO_2 and H_2O. To successfully integrate all the heat exchangers, the Energy Analysis tool of Aspen Plus® has been applied to the final simulation. No limitation of number nor size of heat exchangers is set and therefore, the suggested solution is the most energetically efficient. Finally, solid-solid heat exchangers between reduced and oxidized ceria were assumed to have an efficiency of 50%, even though this equipment is still under development [55]. In Figure 4, the solid-solid heat exchangers are depicted with units E-102 and E-202.

Waste heat at high temperatures (>600 °C) is obtained in several parts of the process, such as exothermal reactors (R-101, R-201 and R-501) and coolers (E-103, E-104, E-203 and E-204). As already suggested by other authors, this heat can be used for powering a Rankine cycle and obtain electricity [56,57]. In large plants, steam Rankine cycles (SRC) are assumed to achieve 40% [58]. In case of smaller decentralized applications, the use of novel organic Rankine cycles (ORC) is recommended, with efficiencies only around 10% [59]. One of the new concepts introduced in this work is emulating co-generation plants and using the heat released in the condenser of the Rankine cycle to directly regenerate the LT-DAC units. However, this idea forces the heat of the condenser to be above 100 °C and thus penalizes the efficiency of the Rankine cycle. The reason is that amongst other variables, efficiency is improved by pressures below 0 barg at the outlet of the turbine, which requires temperatures below 100 °C in the condenser. To quantify the impact of this approach, a model of a steam Rankine cycle has been built in Aspen Plus® with physical parameters from APV100.PURE36 Databank and the property method "ASME 1967 steam table correlations" (STEAM-TA). Typical subcritical conditions of 538 °C and 163 bar at the inlet and an isentropic efficiency of 90% were assumed for the turbine [60]. The complete flowsheet and stream table can be found in Supplementary Materials.

2.3.3. Water Desalination

For the present study, solar multi-effect distillation has been suggested as a solution for desalinating seawater in those scenarios that have a net positive water need. The associated thermal and electric energy requirements per cubic meter of desalinated water are estimated to be 5.50 kWh/m^3 and 1.75 kWh/m^3, respectively [61]. The water needs considered are the consumption (or production) of the DAC unit, the input for hydrogen production and the cleaning of the heliostats. According to available estimations, the latter depends on the heliostat surface and requires 58 L/m^2/y [62]. Additionally, no refrigeration water is necessary since air is set as the only possible cooling utility and no

cost distinctions are made between different water purities, although it should be noted that water fed to the WS reactor must be highly purified if compared to the process or cleaning water.

2.4. Considered Scenarios

A total of five scenarios were identified with synergies that include heat and process integration, as well as use of by-products. Then, improvements are quantified against each other and a baseline in which no synergies between DAC and synthetic fuel production are implemented. The metric used will be solar-to-fuel efficiency (η_{StF}) at steady state and at nominal power of the equipment as defined in Equation (10). The auxiliary heat input (Q_{aux}) in Equation (11) only applies to those scenarios that require natural gas or electricity from support renewable energies (e.g., PV). These renewable energies are assumed to have an efficiency of 20% [25]. The techno-economic analysis of the presented scenarios and transient simulations is out of scope.

$$\eta_{StF} = \frac{\dot{m}_{MeOH} \times HHV_{MeOH}}{\frac{\dot{Q}}{\eta_{opt}} + \dot{Q}_{aux}} \tag{10}$$

$$\dot{Q}_{aux} = \dot{m}_{CH_4} \times LHV_{CH_4} + \frac{\dot{W}_{el}}{\eta_{RE}} \tag{11}$$

The five considered scenarios are described in Figure 5 and Table 2 alongside with the baseline. Moreover, a more detailed summary of the inputs and assumptions for each scenario can be seen in Table S3 in Supplementary Materials. For large-scale approaches (Baseline and Scenarios A to D), a 660 MWth central receiver will be assumed. This unit is equivalent to the Moroccan plant NOOR III, with a heliostat field of 1.3 km^2 [63]. In the decentralized configuration (Scenario E), a solar dish receiver equivalent to the ones used in Maricopa solar project will be used to reduce the unit's size. According to published data, the thermal power of this type of solar dish is 48.1 kWth [64]. For both receivers, an optical efficiency of 60% is assumed based on available measurements [65,66].

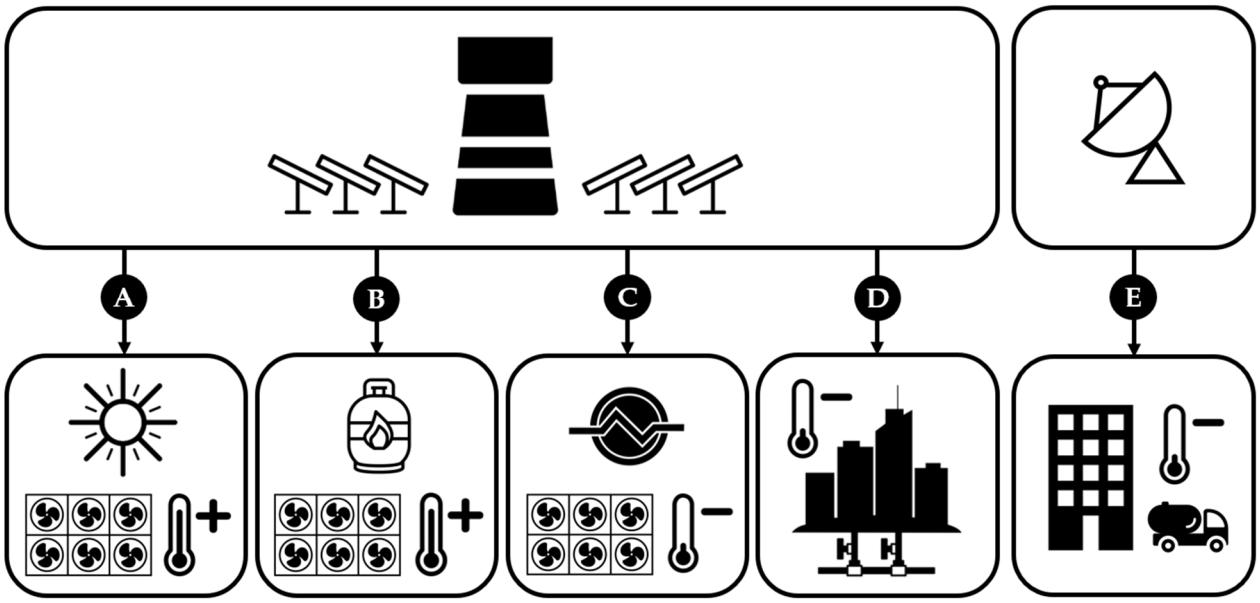

Figure 5. Overview of the five scenarios showing the concentrated solar thermal energy (CSTE) approach used in the upper part and the direct air capture (DAC) strategy in the lower part.

Table 2. Description of the five considered scenarios and comparison with baseline. The terms "Co-generation (DAC)" and "Co-generation (District Heat)" refer to directly using the heat of the condenser to regenerate the LT-DAC units or to power a district heating grid, respectively. ASU means air separation unit, while HVAC stands for heating, ventilation and air conditioning. The acronyms SRC and ORC refer to steam and organic Rankine cycle, respectively.

-	Baseline	A. Central sHT	B. Central HT	C. Central LT	D. Hybrid LT	E. Decentralized
Solar Input	Central receiver	Central receiver	Central receiver	Central receiver	Central receiver	Solar dish
DAC	HT-DAC (O_2 from ASU)	sHT-DAC	HT-DAC (O_2 from TCC)	LT-DAC	LT-DAC in HVAC	LT-DAC in HVAC
CO_2 Treatment	Compression + Transport	-	-	-	Compression + Transport	Compression
Waste heat use	-	SRC	SRC	Co-generation (DAC)	Co-generation (District Heat)	LT-DAC and ORC

As previously mentioned, the baseline does not include any integration between DAC and synthetic fuel production processes. It uses HT-DAC and releases the waste heat to the environment. In scenarios A and B, waste heat is used for producing electricity with an SRC, and no treatment of CO_2 is needed thanks to the integration of processes. The difference between Scenarios A and B is the DAC technology used: the former relies on sHT-DAC, whereas the latter uses HT-DAC. In contrast, Scenario C captures CO_2 with LT-DAC and thanks to the lower temperature requirement, it is able to use the waste heat in a co-generation plant to produce electricity and regenerate the CO_2 capture unit. Although using the same DAC technology, Scenario D outsources the capture of CO_2 to a network of buildings that have integrated the LT-DAC in their HVAC systems. In this case, the waste heat is used to power a district heating grid. The logic behind this is that buildings could use this district heating for regenerating the carbon capture units, thus avoiding overloading the energy grid. Finally, Scenario E is fully decentralized and produces synthetic fuels at the same building where CO_2 is captured. As a consequence, its production is several orders of magnitude lower. It uses its waste heat for the direct regeneration of the LT-DAC. The remaining heat is converted to electricity with an ORC.

3. Results and Discussion

3.1. DAC: Energy and Water Consumption

First, the energy and water consumption of DAC was calculated for each described scenario considering the impact of the synergies, and the results are shown in Figure 6. In the figure, it can be seen that the configuration with the lowest heat consumption is Scenario A thanks to the more efficient sHT-DAC approach. When it comes to electricity, the Baseline has the highest consumption, partly because an ASU unit is required. According to the calculations, the oxygen obtained as a by-product in the TCC doubles the needs for producing the oxyfuel mix used in scenario B, which means that no ASU needs to be powered. Scenario A also avoids the ASU thanks to the solar calcination. In addition, since no additional CO_2 from natural gas combustion needs to be captured, Scenario A is substantially more efficient than the conventional HT-DAC approach. It should also be noted that although Scenario D relies on the same technology as scenarios C and E, it shows a neutral point in the plot because it is assumed that no water collected via LT-DAC is transported from the urban areas to the plant.

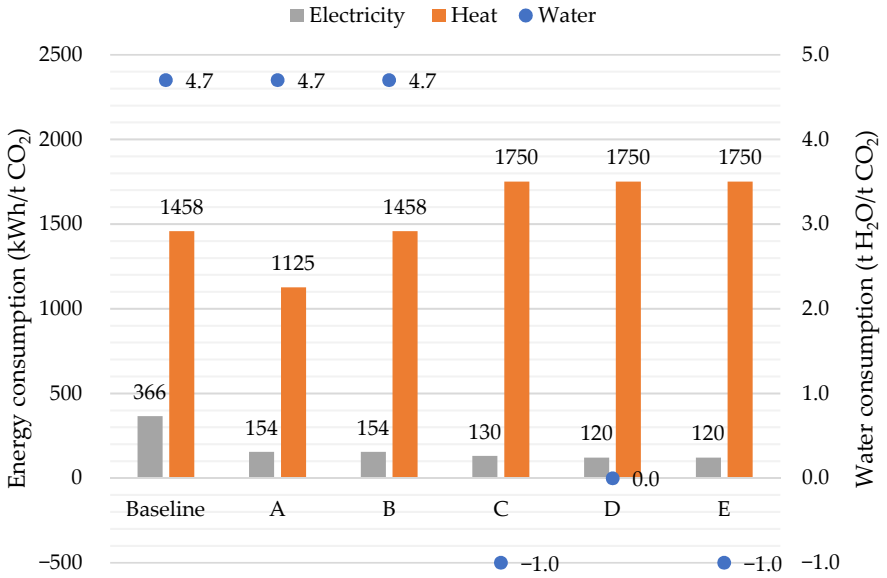

Figure 6. DAC electricity, heat and water consumption for each scenario with applied synergies. Negative values in water column show excess water production.

3.2. Synthetic Fuel Production: Energy Consumption

Second, the results of the synthetic fuel production section are presented in Table 3. This part of the model is not directly affected by synergies, and therefore, it applies to all the scenarios and baseline.

Table 3. Summary of the results for the synthetic fuel production model, which are valid for all scenarios.

Parameter	Units	Value
Solar heat input	kWh/t CO_2	27,194
Waste heat (>500 °C)	kWh/t CO_2	3290
Electricity needed	kWh/t CO_2	746
Water input	t H_2O/t CO_2	568
Methanol produced	kg/t CO_2	728

The energetic assessment of the different separation alternatives for the CO/CO_2 mixture at the outlet of the CDS reactor (Figure 7) showed that liquid absorption was the most efficient technology at the CO concentrations obtained with a 40% conversion. However, VPSA might also be an interesting alternative at low CO concentrations. Interestingly, the suggested approach of integrating the CO/CO_2 separation with the HT-DAC unit becomes the most efficient option at CO molar concentrations above 0.75. From all the different DAC technologies, sHT-DAC was chosen as it was the most energy efficient. Given that each process has different thermal and electrical needs, electricity was assumed to be supplied by a Rankine cycle with a 40% efficiency to allow for comparison. It should also be noted that at very high CO concentrations, and as long as the methanol synthesis catalyst is not poisoned by CO_2, it might be preferable to treat non-reacted CO_2 as an inert gas and purge it downstream.

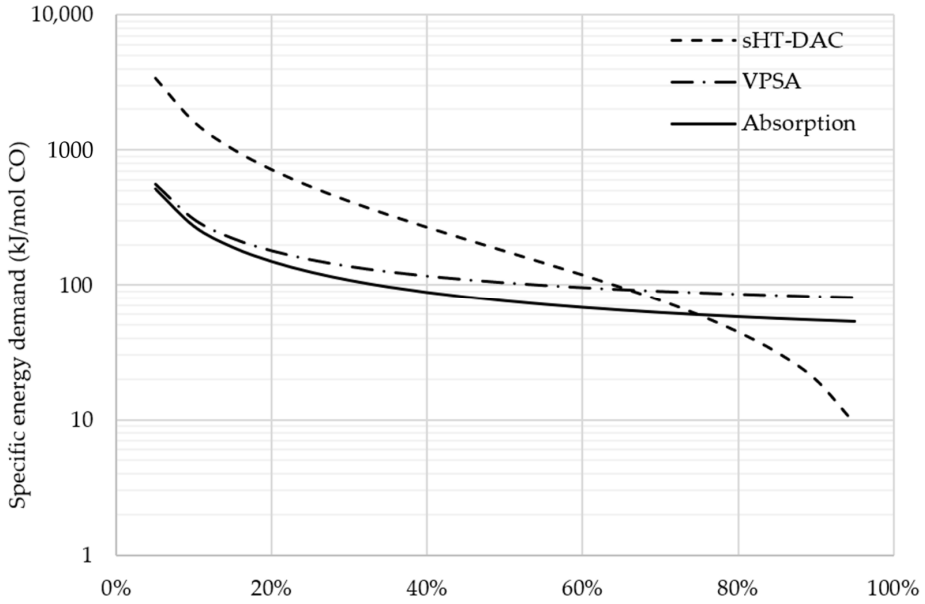

Figure 7. Comparison of the energetic needs required by different CO/CO_2 separation techniques. Electricity has been converted into heat assuming that it is supplied by a Rankine cycle with a 40% efficiency. The acronym VPSA stands for vacuum-pressure swing absorption.

To produce the target vacuum of 5×10^{-4} bar, a system composed of two stages of steam jets and a liquid ring pump is used. The steam is produced at 13 bar using the waste heat available from other sections of the process. The energetic needs of this system are shown in Table 4.

Table 4. Energy requirements of the vacuum system. In the titles, SJ-1 and SJ-2 stand for steam jet 1 and 2, respectively, while LRP means liquid ring pump.

Parameter	Units	SJ-1	SJ-2	LRP
Pressure at inlet	mbar	0.5	5	50
Pressure at outlet	mbar	5	50	1000
Steam	kg/kmol O_2	172	561	-
Electricity	kWh/kmol O_2	-	-	6.09

The significant increment in steam consumption in the second steam jet stage is caused by the fact that steam condensation between stages is unfeasible at 5 mbar since it would take place at temperatures below 0 °C. Therefore, the second stage must pump the removed oxygen as well as the steam from the first stage. The outlet pressure of the second stage allows for the condensation of the steam, thus reducing the electricity consumption of the liquid ring pump.

3.3. Comparison between Sweep Gas and Vacuum

Regarding the use of sweep gas, vacuum or a combination of both in the reduction reactor, the results show that the energy needed for pumping the large flowrates of nitrogen outweighs the vacuum savings. This phenomenon can be seen in Figure 8, where a comparison between using exclusively sweep gas or vacuum to achieve a certain oxygen partial pressure is depicted. Combinations of vacuum and sweep gas are possible, but would be placed between the lines, thus leading to suboptimal solutions. Therefore, it is safe to state that vacuum is the most energy-efficient solution for obtaining low oxygen partial pressures if sweep gas is not recycled.

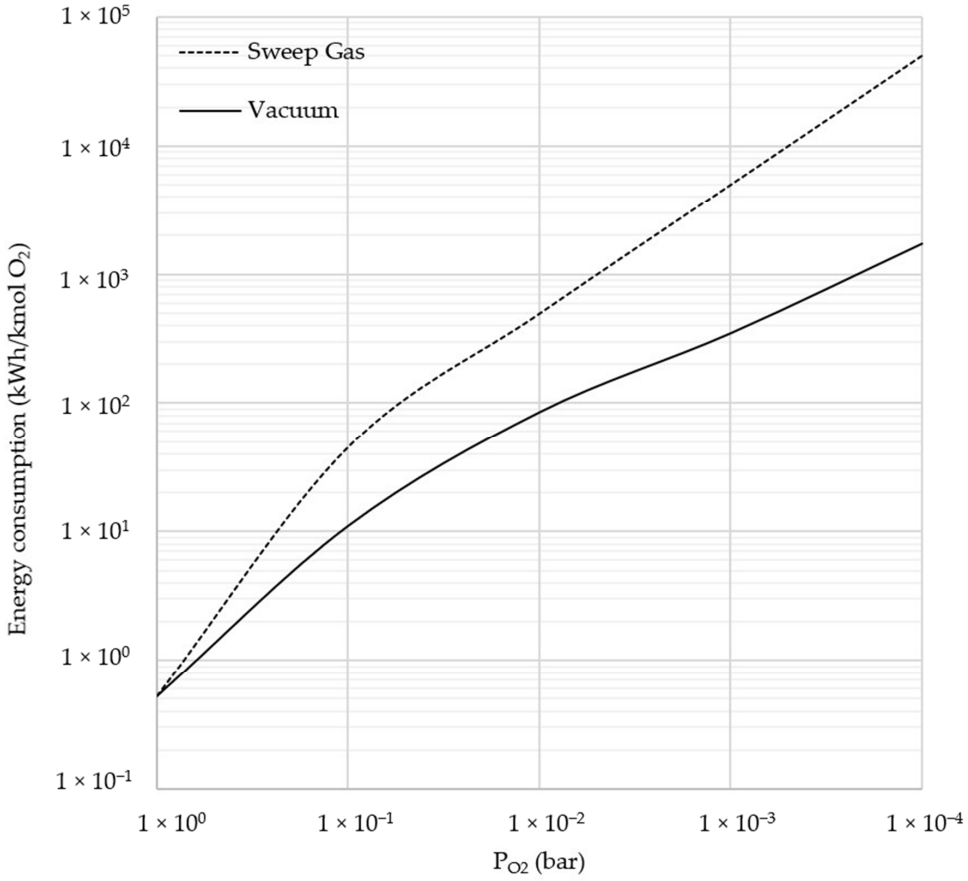

Figure 8. Energy consumption per mole of oxygen released to the atmosphere as a function of oxygen partial pressure (P_{O2}). The dotted line represents the use of sweep gas with different purities under constant atmospheric pressure. The solid line shows the use of different vacuum pressures without sweep gas.

However, in case that high purity sweep gas is used to achieve low oxygen partial pressures, the outlet of the reduction reactor would still contain considerably low amounts of oxygen. In this case, it could be more efficient to treat and recycle the gas rather than directly releasing it to the atmosphere. This situation is analyzed in Figure 9, where a total pressure drop of 100 mbar along the circuit has been assumed, as well as a reduced purification cost (i.e. 25% of the energy needed by an ASU). As the reader will notice, vacuum is still the most efficient solution for high (>0.1 bar) and very low ($<1 \times 10^{-3}$ bar) oxygen partial pressures, although using only sweep gas is significantly more efficient than it was without recycling. Contrary to Figure 8, combinations of sweep gas and vacuum are not entirely found between vacuum and sweep gas lines. In fact, a combination of sweep gas ($x_{O2} = 0.1$) and vacuum ($P_{red} = 0.1$ bar) is preferable for oxygen partial pressures of 0.01 bar. This exception is caused by the combination of relatively low nitrogen flows and a moderate vacuum, which can be provided without the steam jets.

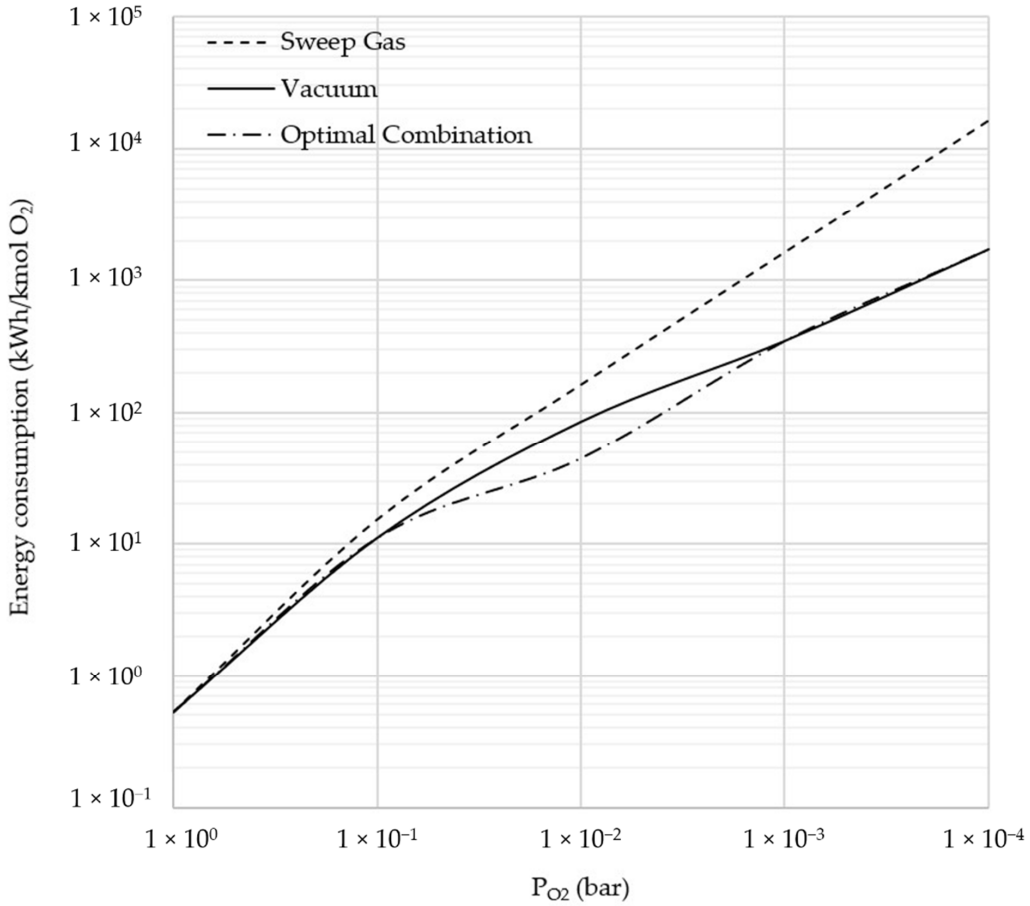

Figure 9. Energy consumption per mole of oxygen removed in a closed circuit of sweep gas as a function of oxygen partial pressure (P_{O2}). The dotted line represents the use of sweep gas with different purities under constant atmospheric pressure, the solid line shows the use of different vacuum pressures without sweep gas and the dash-dotted line depicts the optimal combination of sweep gas and vacuum. The global pressure drop is assumed to be 100 mbar and the purification energy requirements, 4 kJ/mol N_2.

3.4. Co-Generation Performance

Scenarios C and D rely on co-generation to use the process residual heat. As described, in scenario C condenser heat is directly consumed in the regeneration of LT-DAC units. Similarly, Scenario D uses it for producing hot water that could be distributed in urban areas with a district heating infrastructure. As observed in Figure 10, the model for the Rankine cycle shows that, if a ΔT of 10 °C between cold and hot sides of the condenser is allowed, the steam should condensate at 110 °C. This means that it must be discharged from the turbine at around 1.5 bar, allowing an overall Rankine efficiency close to 28%. Calculations also show, that heat supplied by the condenser cannot exceed 60% of the waste heat fed to the cycle. Given that scenario E is using an organic Rankine cycle (ORC), the temperatures at the condenser are too low for LT-DAC regeneration. As a solution, the decentralized approach directly uses the waste heat at high temperatures at expense of electricity production.

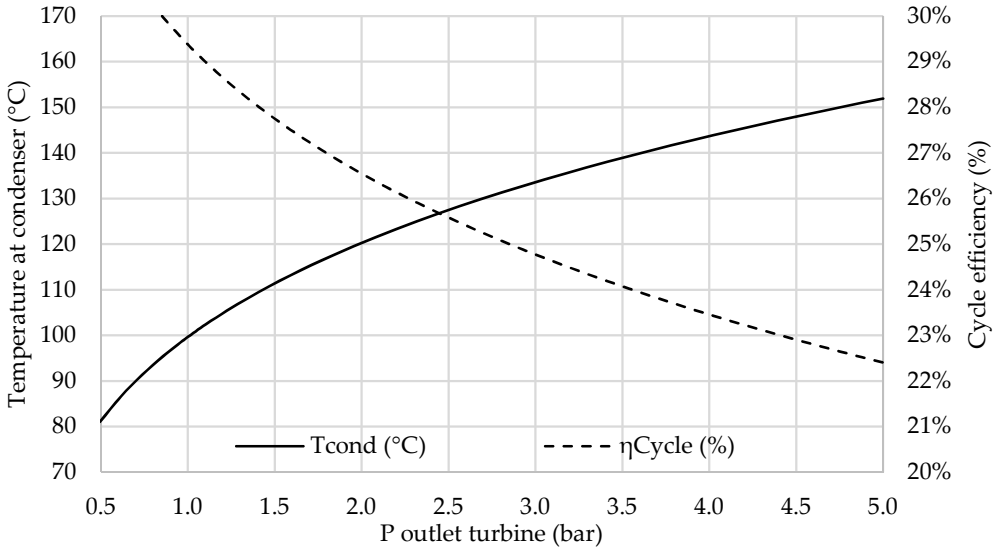

Figure 10. Temperature at the condenser of the Rankine cycle (T_{cond}, left axis) and cycle efficiency (η_{Cycle}, right axis) as a function of turbine's discharge pressure.

3.5. Overall Results

Overall electricity and water needs are calculated and shown in Figure 11. For further information on the calculations performed, a summary is shown in Table S3 in Supplementary Materials. From all the scenarios, C and E are the only ones in which no water desalination is needed because it is produced at a higher rate than consumed thanks to the LT-DAC. Subsequently, they are the lowest values in the plot. Water is also obtained in Scenario D, but since storing and transportation of CO_2 must be carried out without free water to avoid corrosion, it is not transported to the production plant. When it comes to electricity, Scenario E must use some energy input from PV panels (or grid if carbon intensity of the mix is low enough) to operate, which is a consequence of the comparatively less efficient ORC. As a consequence, Scenario E shows the second highest electricity consumption, only after the baseline. From their lowest position in the figure, it is also clear that Scenarios A and B are producing more electricity than C and D thanks to a conventional Rankine cycle without co-generation that operates at higher efficiency.

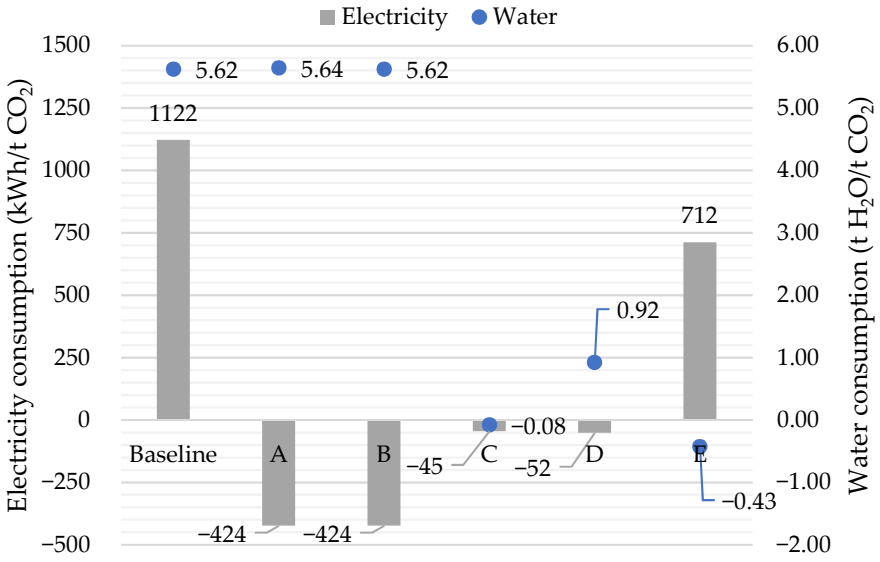

Figure 11. Global electricity and water consumption or production of each scenario.

The main data result, the solar-to-fuel efficiency, is calculated and shown in Figure 12 for each scenario. Similarly, further information about its calculation is available in Table S3 in Supplementary Materials. Scenarios C and D are tied and show the highest efficiency of 10.2%, which is 1.4 percentage points higher than the baseline. Below, Scenarios A and B present similar efficiencies at 9.8% and 9.9%, respectively. Scenario E closes the ranking with a 9.5% efficiency, but it still lays 0.7 points above baseline.

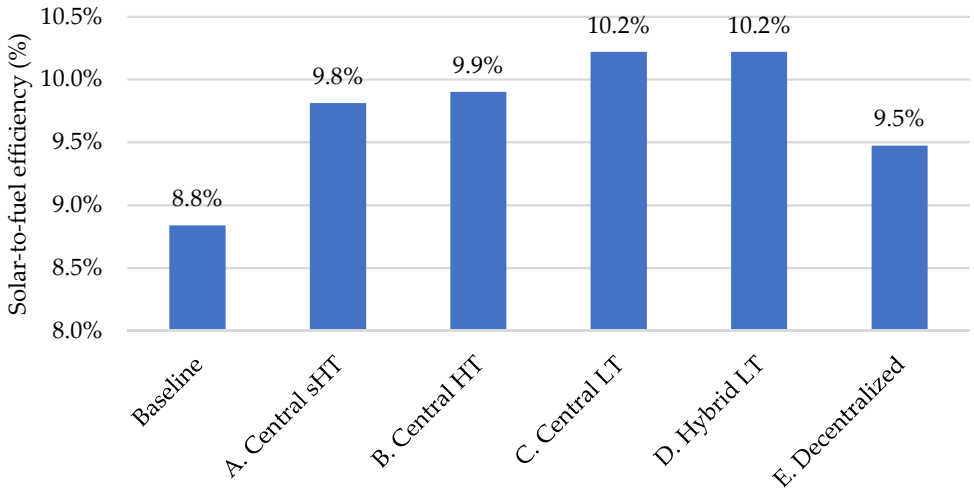

Figure 12. Comparison of solar-to-fuel efficiency for each scenario and baseline.

3.6. Sensitivity Analysis: Lower Oxygen Partial Pressure

The technology described in Section 2.3.1 would allow reaching higher reduction extents and thus, lower ceria flowrates would be needed. This would be translated into lower heat losses and cheaper equipment. However, results show that this improvement may not be beneficial for all suggested scenarios. As it can be seen in Figure 13, Scenarios C and D suffer in fact a reduction of their solar-to-fuel efficiency, while scenarios A and B become the most competitive configurations. It is also remarkable that the baseline efficiency is especially enhanced since it increases by more than one percentage point.

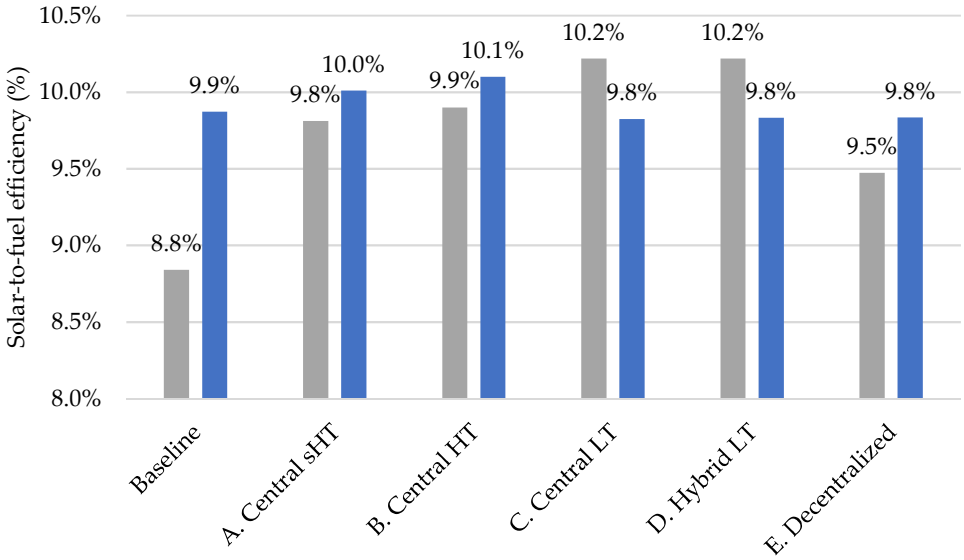

Figure 13. Impact of a hypothetical reduction of oxygen partial pressure in the reduction step on the solar-to-fuel efficiency of each scenario. Above each scenario, two bars are shown: gray bars (left) show the previous values and blue bars (right), the recalculated efficiencies.

This phenomenon can be better explained with Figure 14, where two Sankey diagrams are used to describe the distribution of energy for Scenario C in the base case ($P_{O2} = 5 \times 10^{-4}$ bar, upper plot) and in the enhanced case ($P_{O2} = 1 \times 10^{-6}$ bar, lower plot). In the base case, the TCC requires more heat because higher flowrates of ceria are necessary at lower reduction extents. Due to the lower efficiency of the solid-solid heat exchangers, a remarkable amount of this heat is converted into steam that is used for powering the steam jets and the Rankine cycle. Thanks to the co-generation concept, the Rankine cycle is able to fully regenerate the LT-DAC and supply more electricity than consumed, thus avoiding the need of a supporting renewable energy.

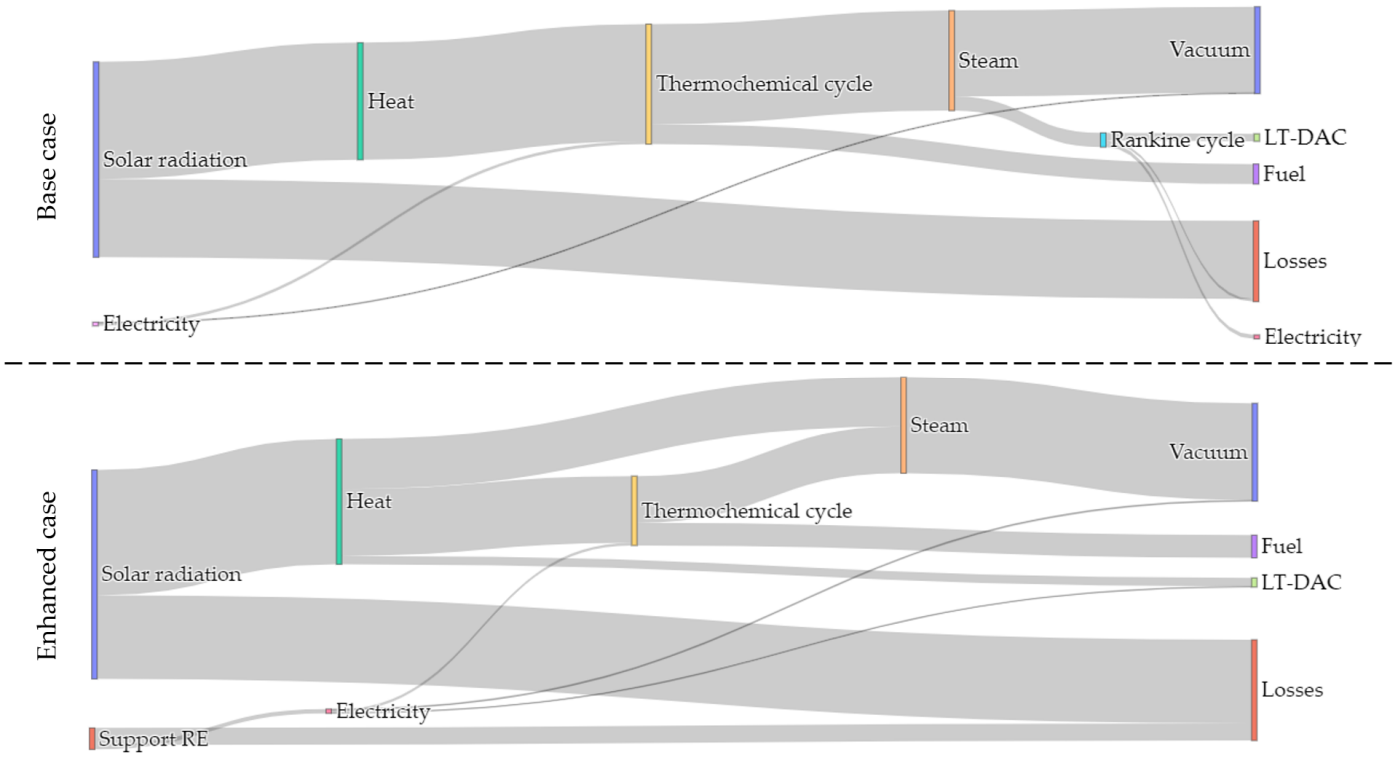

Figure 14. Sankey diagrams for Scenario C in the base case ($P_{O2} = 5 \times 10^{-4}$ bar, upper plot) and in the enhanced case ($P_{O2} = 1 \times 10^{-6}$ bar, lower plot). The term "Support RE" stands for support renewable energy (e.g., PV).

In contrast, lower ceria flowrates are required for the TCC in the enhanced case, and therefore, less waste heat is produced. However, the obtained steam from this waste heat is not enough for the vacuum system, which has two consequences: first, part of the CSTE must be used for meeting the steam demand and regenerating the LT-DAC, and second, a supporting renewable energy must be introduced to supply the required electricity. Alternatively, the plant could also be connected to the power grid.

4. Conclusions

Although the system analyzed in this work is unparalleled, the obtained efficiencies in the range of 8.8 to 10.2% are consistent with other studies in the field that use similar Aspen Plus® models [15,41]. If compared to research performed with different methodology, the highest experimental efficiency reported for a TCC is 5.25% [43]. Moreover, system efficiencies as high as 38.2% have been published when using less conservative models in different software [56,57].

Results show that Scenarios C and D are the most efficient approaches with a solar-to-fuel efficiency of 10.2%. However, Scenario C does not need desalination and thus could be more suitable for dry areas without sea access. Collected data also discourages the use of HT-DAC or sHT-DAC technologies in such locations. Therefore, it seems safe to state

that configurations in Scenarios A and B should be operated close to an abundant water source or in areas with relatively high air moisture. The Scenarios D and E could become an asset for achieving more sustainable cities, but their integration would be arguably more expensive due to the required collection infrastructure of CO_2 (Scenario D) or methanol (Scenario E). Nevertheless, a techno-economical assessment should be carried out in future works to complement these recommendations.

This study also shows that a Rankine cycle with co-generation (which is implemented in Scenarios C and D) substantially improves solar-to-fuel efficiency and, therefore, could be the most remarkable synergy between DAC and synthetic fuels production.

It must be also highlighted that generation of low oxygen partial pressure is one of the main energy consumers. Although a lower oxygen partial pressure without additional energy expenses would minimize the equipment cost, it also reduces the benefits of the synergies by penalizing Scenarios C and D and boosting baseline efficiency. The reason behind is that the most powerful synergies explored in this study are focused on the waste heat exploitation. Therefore, similar consequences should be expected with a more efficient solid-solid heat exchange.

Based on the outcome of this work, any future improvement in the fields of vacuum production and metal oxide research would have remarkable consequences on the presented technology. These advances would allow either a higher reduction extend with the same energy consumption or maintaining the reduction extend at lower temperatures. The latter is especially promising because, to date, no mature thermal storage system can supply heat at 1500 °C. Therefore, a lower reduction temperature alongside with progresses in heat storage could open the door to the operation of a TCC with stored heat. As a consequence, the production of synthetic fuels would be possible around the clock, thus boosting the yearly hours of operation and reducing the cost of solar synthetic fuels.

Supplementary Materials: The following are available online at https://www.mdpi.com/article/10.3390/en14164818/s1, Figure S1: Flowsheet of the Aspen Plus® simulation of synthetic fuel production, Figure S2: Flowsheet of the Aspen Plus® simulation of the steam Rankine cycle, Table S1: Stream information of the Aspen Plus® simulation of synthetic fuel production, Table S2: Stream information of the Aspen Plus® simulation of the steam Rankine cycle, Table S3: Summary of inputs and results for each scenario.

Author Contributions: Conceptualization, E.P.-S. and N.M.; funding acquisition, C.S.; investigation, E.P.-S.; project administration, N.M.; software, E.P.-S.; supervision, N.M.; writing—original draft, E.P.-S.; writing—review and editing, E.P.-S. and N.M. All authors have read and agreed to the published version of the manuscript.

Funding: This research was funded by the German Helmholtz Gemeinschaft research centers (HGF) Klimainitiative (HI-CAM: Helmholtz-Initiative Climate Adaptation and Mitigation).

Institutional Review Board Statement: Not applicable.

Informed Consent Statement: Not applicable.

Data Availability Statement: No new data were created or analyzed in this study. Data sharing is not applicable to this article.

Conflicts of Interest: The authors declare no conflict of interest. The funders had no role in the design of the study; in the collection, analyses, or interpretation of data; in the writing of the manuscript, or in the decision to publish the results.

References

1. Lüthi, D.; Le Floch, M.; Bereiter, B.; Blunier, T.; Barnola, J.-M.; Siegenthaler, U.; Raynaud, D.; Jouzel, J.; Fischer, H.; Kawamura, K.; et al. High-resolution carbon dioxide concentration record 650,000–800,000 years before present. *Nature* **2008**, *453*, 379–382. [CrossRef] [PubMed]
2. Plass, G.N. The Carbon Dioxide Theory of Climatic Change. *Tellus* **1956**, *8*, 140–154. [CrossRef]
3. Blunden, J.; Arndt, D.S. State of the Climate in 2019. *Bull. Am. Meteorol. Soc.* **2020**, *101*, S1–S429. [CrossRef]

4. Edenhofer, O. (Ed.) *Climate Change 2014: Mitigation of Climate Change Working Group III Contribution to the Fifth Assessment Report of the Intergovernmental Panel on Climate Change*; Cambridge University Press: New York, NY, USA, 2014; ISBN 978-1-107-05821-7.
5. *The Emissions Gap Report 2020*; United Nations Environment Programme: Nairobi, Kenya, 2020; ISBN 978-92-807-3812-4.
6. Dittmeyer, R.; Klumpp, M.; Kant, P.; Ozin, G. Crowd oil not crude oil. *Nat. Commun.* **2019**, *10*, 1–8. [CrossRef]
7. Brady, C.; Davis, M.E.; Xu, B. Integration of thermochemical water splitting with CO2 direct air capture. *Proc. Natl. Acad. Sci. USA* **2019**, *116*, 25001–25007. [CrossRef]
8. Agrafiotis, C.; Roeb, M.; Sattler, C. 4.18 Solar Fuels. In *Comprehensive Energy Systems*; Dincer, I., Ed.; Elsevier: Amsterdam, The Netherlands, 2018; ISBN 978-0-12-814925-6.
9. Götz, M.; Lefebvre, J.; Mörs, F.; Koch, A.M.; Graf, F.; Bajohr, S.; Reimert, R.; Kolb, T. Renewable Power-to-Gas: A technological and economic review. *Renew. Energy* **2016**, *85*, 1371–1390. [CrossRef]
10. Pregger, T.; Schiller, G.; Cebulla, F.; Dietrich, R.-U.; Maier, S.; Thess, A.; Lischke, A.; Monnerie, N.; Sattler, C.; Le Clercq, P.; et al. Future Fuels—Analyses of the Future Prospects of Renewable Synthetic Fuels. *Energies* **2020**, *13*, 138. [CrossRef]
11. Stechel, E.B.; Miller, J.E. Re-energizing CO_2 to fuels with the sun: Issues of efficiency, scale and economics. *J. CO_2 Util.* **2013**, *1*, 28–36. [CrossRef]
12. Miller, J.E. *Initial Case for Splitting Carbon Dioxide to Carbon Monoxide and Oxygen*; Sandia National Laboratories: Albuquerque, NM, USA; Livermore, CA, USA, 2007.
13. Irena and Methanol Institute. *Innovation Outlook: Renewable Methanol*; International Renewable Energy Agency: Abu Dhabi, United Arab Emirates, 2021.
14. Basile, A.; Dalena, F. *Methanol: Science and Engineering*; Elsevier: Amsterdam, The Netherlands, 2017; ISBN 9780444639035.
15. Kim, J.; Johnson, T.A.; Miller, J.E.; Stechel, E.B.; Maravelias, C.T. Fuel production from CO_2 using solar-thermal energy: System level analysis. *Energy Environ. Sci.* **2012**, *5*, 8417–8429. [CrossRef]
16. Scheffe, J.R.; Steinfeld, A. Thermodynamic Analysis of Cerium-Based Oxides for Solar Thermochemical Fuel Production. *Energy Fuels* **2012**, *26*, 1928–1936. [CrossRef]
17. Lua, Y.; Zhua, L.; Agrafiotis, C.; Vieten, J.; Roeb, M.; Sattler, C. Solar fuels production: Two-step thermochemical cycles with cerium-based oxides. *Progess Energy Combust. Sci.* **2019**, *75*, 100785. [CrossRef]
18. Rytter, E.; Souskova, K.; Lundgren, M.K.; Ge, W.; Nannestad, A.D.; Venvik, H.J.; Hillestad, M. Process concepts to produce syngas for Fischer–Tropsch fuels by solar thermochemical splitting of water and/or CO_2. *Fuel Process. Technol.* **2016**, *145*, 1–8. [CrossRef]
19. Brendelberger, S.; von Storch, H.; Bulfin, B.; Sattler, C. Vacuum pumping options for application in solar thermochemical redox cycles–Assessment of mechanical-, jet- and thermochemical pumping systems. *Sol. Energy* **2017**, *141*, 91–102. [CrossRef]
20. Bulfin, B.; Lapp, J.; Richter, S.; Gubàn, D.; Vieten, J.; Brendelberger, S.; Roeb, M.; Sattler, C. Air separation and selective oxygen pumping via temperature and pressure swing oxygen adsorption using a redox cycle of $SrFeO_3$ perovskite. *Chem. Eng. Sci.* **2019**, *203*, 68–75. [CrossRef]
21. Bulfin, B.; Call, F.; Lange, M.; Lübben, O.; Sattler, C.; Pitz-Paal, R.; Shvets, I.V. Thermodynamics of CeO_2 Thermochemical Fuel Production. *Energy Fuels* **2015**, *29*, 1001–1009. [CrossRef]
22. Steinfeld, A.; Palumbo, R. Solar Thermochemical Process Technology: Encyclopedia of Physical Science & Technology. In *Encyclopedia of Physical Science and Technology*, 3rd ed.; Meyers, R.A., Ed.; Academic: San Diego, CA, USA; London, UK, 2002; pp. 237–256, ISBN 9780122274107.
23. World Bank. *Concentrating Solar Power: Clean Power on Demand 24/7*; World Bank: Washington DC, USA, 2020.
24. International Energy Agency. *Technology Roadmap: Solar Thermal Electricity*; International Energy Agency: Paris, France, 2014.
25. Trieb, F.; Schillings, C.; O'Sullivan, M.; Pregger, T. Global Potential of Concentrating Solar Power. In Proceedings of the SolarPACES Conference, Berlin, Germany, 15–18 September 2009.
26. Lewis, N.S.; Nocera, D.G. Powering the planet: Chemical challenges in solar energy utilization. *Proc. Natl. Acad. Sci. USA* **2006**, *103*, 15729–15735. [CrossRef]
27. Hanna, R.; Abdulla, A.; Xu, Y.; Victor, D.G. Emergency deployment of direct air capture as a response to the climate crisis. *Nat. Commun.* **2021**, *12*, 1–3. [CrossRef]
28. Deutz, S.; Bardow, A. Life-cycle assessment of an industrial direct air capture process based on temperature—Vacuum swing adsorption. *Nat. Energy* **2021**, *6*, 203–213. [CrossRef]
29. Eisaman, M.D.; Rivest, J.L.; Karnitz, S.D.; Lannoy, C.-F.; de Jose, A.; DeVaul, R.W.; Hannun, K. Indirect ocean capture of atmospheric CO2: Part II. Understanding the cost of negative emissions. *Int. J. Greenh. Gas Control.* **2018**, *70*, 254–261. [CrossRef]
30. Patterson, B.D.; Mo, F.; Borgschulte, A.; Hillestad, M.; Joos, F.; Kristiansen, T.; Sunde, S.; van Bokhoven, J.A. Renewable CO_2 recycling and synthetic fuel production in a marine environment. *Proc. Natl. Acad. Sci. USA* **2019**, *116*, 12212–12219. [CrossRef]
31. Fasihi, M.; Efimova, O.; Breyer, C. Techno-economic assessment of CO_2 direct air capture plants. *J. Clean. Prod.* **2019**, *224*, 957–980. [CrossRef]
32. Keith, D.; Holmes, G.; St. Angelo, D.; Heidel, K. A Process for Capturing CO_2 from the Atmosphere. *Joule* **2018**, *2*. [CrossRef]
33. Gebald, C.; Wurzbacher, J.A.; Tingaut, P.; Zimmermann, T.; Steinfeld, A. Amine-Based Nanofibrillated Cellulose As Adsorbent for CO_2 Capture from Air. *Environ. Sci. Technol.* **2011**, *45*, 9101–9108. [CrossRef] [PubMed]
34. Moumin, G.; Ryssel, M.; Zhao, L.; Markewitz, P.; Sattler, C.; Robinius, M.; Stolten, D. CO_2 emission reduction in the cement industry by using a solar calciner. *Renew. Energy* **2019**, *145*, 1578–1596. [CrossRef]

35. Heß, D.; Klumpp, M.; Dittmeyer, R. *Nutzung von CO2 aus Luft als Rohstoff für synthetische Kraftstoffe und Chemikalien: Studie im Auftrag des Ministeriums für Verkehr Baden-Württemberg*; Ministerium für Verkehr Baden-Württemberg: Stuttgart, Germany, 2020.
36. Viebahn, P.; Scholz, A.; Zelt, O. The Potential Role of Direct Air Capture in the German Energy Research Program—Results of a Multi-Dimensional Analysis. *Energies* **2019**, *12*, 3443. [CrossRef]
37. Wurzbacher, J.A.; Gebald, C.; Piatkowski, N.; Steinfeld, A. Concurrent Separation of CO2 and H2O from Air by a Temperature-Vacuum Swing Adsorption/Desorption Cycle. *Environ. Sci. Technol.* **2012**, *46*, 9191–9198. [CrossRef]
38. Algarni, S.; Saleel, C.A.; Mujeebur, M.A. Air-conditioning condensate recovery and applications—Current developments and challenges ahead. *Sustain. Cities Soc.* **2018**, *37*, 263–274. [CrossRef]
39. Hassan, N.M.; Bakry, A.S. Feasibility of Condensate Recovery in Humid Climates. *Int. J. Archit. Eng. Constr.* **2013**, *2*, 271–279. [CrossRef]
40. Monnerie, N.; Gan, P.G.; Roeb, M.; Sattler, C. Methanol production using hydrogen from concentrated solar energy. *Hydrog. Energy Publ.* **2020**, *45*, 26117–26125. [CrossRef]
41. Kim, J.; Henao, C.A.; Johnson, T.A.; Dedrick, D.E.; Miller, J.E.; Stechel, E.B.; Maravelias, C.T. Methanol production from CO_2 using solar-thermal energy: Process development and techno-economic analysis. *Energy Environ. Sci.* **2011**, *4*, 3122. [CrossRef]
42. Romero, M.; Gonzalez-Aguilar, J.; Sizmann, A.; Batteiger, V.; Steinfeld, A.; Zoller, S.; Brendelberger, S.; Lieftink, D. Solar-Driven Thermochemical Production of Sustainable Liquid Fuels from H_2O and CO_2 in a Heliostat Field. In Proceedings of the ISES SWC2019/SHC2019, Santiago, Chile, 4–7 November 2009; International Solar Energy Society: Freiburg, Germany, 2019.
43. Marxer, D.; Furler, P.; Takacs, M.; Steinfeld, A. Solar thermochemical splitting of CO_2 into separate streams of CO and O_2 with high selectivity, stability, conversion, and efficiency. *Energy Environ. Sci.* **2017**, *10*, 1142–1149. [CrossRef]
44. Lim, Y.-I.; Choi, J.; Moon, H.-M.; Kim, G.-H. Techno-economic Comparison of Absorption and Adsorption Processes for Carbon Monoxide (CO) Separation from Linze-Donawitz Gas (LDG). *Korean Chem. Eng. Res.* **2015**, *54*, 320–331. [CrossRef]
45. Dutta, N.N.; Patil, G.S. Developments in CO separation. *Gas Sep. Purif.* **1995**, *9*, 277–283. [CrossRef]
46. Poudel, J.; Choi, J.H.; Oh, S.C. Process Design Characteristics of Syngas (CO/H_2) Separation Using Composite Membrane. *Sustainability* **2019**, *11*, 703. [CrossRef]
47. Gao, F.; Wang, S.; Wang, W.; Duan, J.; Dong, J.; Chen, G. Adsorption separation of CO from syngas with CuCl@AC adsorbent by a VPSA process. *RSC Adv.* **2018**, *8*, 39362–39370. [CrossRef]
48. Keller, A.; Schendel, R. The Use of COSORB II to Recover High Purity Carbon Monoxide from a Feed Gas. In Proceedings of the AIChE Summer Meeting, Denver, CO, USA, 21–24 August 1988; American Institute of Chemical Engineers: New York, NY, USA, 1988.
49. Peletiri, S.P.; Rahmanian, N.; Mujtaba, I.M. CO_2 Pipeline Design: A Review. *Energies* **2018**, *11*, 184. [CrossRef]
50. Morland, B.H.; Dugstad, A.; Svenningsen, G. Corrosion of Carbon Steel in Dense Phase CO_2 with Water above and Below the Solubility Limit. *Energy Procedia* **2017**, *114*, 6752–6765. [CrossRef]
51. Elvers, B.; Ullmann, F. *Ullmann's Encyclopedia of Industrial Chemistry*, 7th ed.; Wiley-VCH: Weinheim, Germany, 2011; ISBN 978-3-527-32943-4.
52. Bader, R.; Venstrom, L.J.; Davidson, J.H.; Lipinski, W. Thermodynamic Analysis of Isothermal Redox Cycling of Ceria for Solar Fuel Production. *Energy Fuels* **2013**, *27*, 5533–5544. [CrossRef]
53. Jousten, K.; Nakhosteen, C.B. *Handbook of Vacuum Technology*, 2nd ed.; Wiley-VCH: Weinheim, Germany, 2016; ISBN 9783527413386.
54. Pein, M.; Agrafiotis, C.; Vieten, J.; Giasafaki, D.; Brendelberger, S.; Roeb, M.; Sattler, C. Redox thermochemistry of Ca-Mn-based perovskites for oxygen atmosphere control inasm solar-thermochemical processes. *Sol. Energy* **2020**, *198*, 612–622. [CrossRef]
55. Holzemer-Zerhusen, P.; Brendelberger, S.; Roeb, M.; Sattler, C. Oxygen Crossover in Solid–Solid Heat Exchangers for Solar Water and Carbon Dioxide Splitting: A Thermodynamic Analysis. *J. Energy Resour. Technol.* **2021**, *143*, 071301. [CrossRef]
56. Budama, V.K.; Johnson, N.G.; McDaniel, A.; Ermanoski, I.; Stechel, E.B. Thermodynamic development and design of a concentrating solar thermochemical water-splitting process for co-production of hydrogen and electricity. *Int. J. Hydrogen Energy* **2018**, *43*, 17574–17587. [CrossRef]
57. Budama, V.K.; Johnson, N.G.; Ermanoski, I.; Stechel, E.B. Techno-economic analysis of thermochemical water-splitting system for Co-production of hydrogen and electricity. *Int. J. Hydrogen Energy* **2021**, *46*, 1656–1670. [CrossRef]
58. Van Putten, H.; Colonna, P. Dynamic modeling of steam power cycles: Part II–Simulation of a small simple Rankine cycle system. *Appl. Therm. Eng.* **2007**, *27*, 2566–2582. [CrossRef]
59. Rahbar, K.; Mahmoud, S.; Al-Dadah, R.K.; Moazami, N.; Mirhadizadeh, S.A. Review of organic Rankine cycle for small-scale applications. *Energy Convers. Manag.* **2016**, *134*, 135–155. [CrossRef]
60. Beér, J.M. High efficiency electric power generation: The environmental role. *Prog. Energy Combust. Sci.* **2007**, *33*, 107–134. [CrossRef]
61. Kaya, A.; Tok, M.; Koc, M. A Levelized Cost Analysis for Solar-Energy-Powered Sea Water Desalination in The Emirate of Abu Dhabi. *Sustainability* **2019**, *11*, 1691. [CrossRef]
62. Falter, C.; Pitz-Paal, R. Water Footprint and Land Requirement of Solar Thermochemical Jet-Fuel Production. *Environ. Sci. Technol.* **2017**, *51*, 12938–12947. [CrossRef]
63. SENER-NOOR III. Available online: https://www.energy.sener/pdf-sener-special/NOORoIII-thermosolar-plant (accessed on 9 July 2021).

64. SolarPACES-Maricopa Solar Project. Available online: https://solarpaces.nrel.gov/maricopa-solar-project (accessed on 22 April 2021).
65. Collado, F.J.; Guallar, J. Quick design of regular heliostat fields for commercial solar tower power plants. *Energy* **2019**, *178*, 115–125. [CrossRef]
66. Dähler, F.; Wild, M.; Schäppi, R.; Haueter, P.; Cooper, T.; Good, P.; Larrea, C.; Schmitz, M.; Furler, P.; Steinfeld, A. Optical design and experimental characterization of a solar concentrating dish system for fuel production via thermochemical redox cycles. *Sol. Energy* **2018**, *170*, 568–575. [CrossRef]